Macromolecules
COMMUNICATION TO THE EDITOR

Macromolecules **2010**, *43*, 4429–4434 **4429**
DOI: 10.1021/ma1003248

Confinement Effects on Chain Dynamics and Local Chain Order in Entangled Polymer Melts

Salim Ok and Martin Steinhart

Institut für Chemie, Universität Osnabrück, Barbarastr. 7, D-46069 Osnabrück, Germany

Anca Şerbescu[†]

Institut für Makromolekulare Chemie, Universität Freiburg, Stefan-Meier-Str. 31, D-79104 Freiburg, Germany [†]*Now at: Dow Europe GmbH, Horgen, Switzerland*

Cornelius Franz, Fabián Vaca Chávez,[‡] **and Kay Saalwächter***

Institut für Physik-NMR, Martin-Luther-Universität Halle-Wittenberg, Betty-Heimann-Str. 7, D-06120 Halle, Germany [‡]*Now at: Universidade de Lisboa, Lisbon, Portugal*

Received February 10, 2010
Revised Manuscript Received April 13, 2010

Introduction. Effects of nanometric confinement on polymer structure and dynamics have been in the focus for more than 15 years, primarily with the aim of providing the physical understanding for nanoscale polymer applications such as in composite materials. Changes in T_g are probably the most researched, but still controversial issue, with clear and intuitively expected indications of slowed-down segmental dynamics for the case of strongly absorbing surfaces but sometimes conflicting trends and a lack of understanding of the physical basis for the often decreased T_g close to free or nonabsorbing interfaces.[1−8] One may expect that potential changes in T_g, being related to the time scale of segmental relaxation, should directly influence also larger scale relaxations. However, even slow mechanical relaxation around T_g and aging processes below T_g appear to bear no simple relation to the observed T_g changes,[9,10] and the reason may be sought in a modified monomer packing persisting over length scales much beyond the radius of gyration (R_g), as seen in computer simulations.[2]

At larger length scales, changes in the whole-chain conformation, as again seen in simulations,[2,4] have been assessed by scattering techniques,[11−15] with most studies concluding no deviation from Gaussian behavior. Nevertheless, the self-concentration is expected to be increased locally since the random walk of a chain close to a neutral interface is reflected onto itself. Consequently, a reduced interchain entanglement density has been discussed as the reason for enhanced flow of confined chains.[15−18] In contrast, a "sticky" surface or local orientation effects and thus anisotropic dynamics of the segments close to an interface are thought to be the reason for enhanced elasticity[19] or reduced diffusion coefficients.[20,21] Interestingly, a slowdown of diffusion has also been reported for chains close to a free surface,[22] in apparent contrast to the (sometimes only transiently) reduced viscosity observed by others.[15,17,18] Annealing and nonequilibrium effects may thus play an important role.[7,18] Note that in all cases the effects were observed in a range up to or even beyond R_g.

In this Communication, we present first results on the degree of anisotropy of segmental orientation fluctuations in entangled and geometrically confined chains in two different types of well-defined model nanocomposites with weakly interacting interfaces. We address temperatures far above T_g and time scales beyond the bulk entanglement time τ_e, providing a molecular-basis view of the discussed phenomena. We use a recently established multiple-quantum (MQ) NMR technique,[23−26] which probes the time-dependent degree of local chain orientation via the monomer-averaged apparent residual dipolar coupling constant, D_{res}. At a given time and temperature, the experimental intensity at short pulse-sequence times τ_{DQ} depends on the square of this quantity; more precisely, it is directly proportional to the orientation autocorrelation function

$$C(t) = \langle P_2(\cos\theta(t)) P_2(\cos\theta(0)) \rangle \qquad (1)$$

where θ is the segmental orientation relative to the external magnetic field. In polymer melts, the decay of $C(t)$ reflects chain motions in the tube-model regimes II−IV,[23,26] and its magnitude $C(\tau_e)^{1/2} \sim 1/N_e$ reflects the macroscopic elasticity in terms of the number of segments in an entangled strand (tube diameter). In networks, $C(t\rightarrow\infty)^{1/2} \sim 1/N_c$ exhibits a long-time plateau that at high cross-link density is directly proportional to the cross-link density.[25]

Our results indicate significantly more anisotropic fluctuations in all confined systems as compared to the bulk. These findings appear related to the "corset effect", which was mainly observed in terms of strong changes of the frequency-dependent T_1 relaxation times of spins (^{1}H, ^{2}H, ^{19}F) in chains under geometric confinement in the nanometer−micrometer range.[27−30] Kimmich et al. concluded these also to be due to highly anisotropic fluctuations, yet while in their work the effect appeared homogeneous throughout the sample, we find qualitative changes of our experimental response functions that indicate an inhomogeneous scenario, and we draw first conclusions on the length scale of the phenomenon.

Results and Discussion. As a first model system to study interface-induced effects on polymer dynamics, we chose the preparation of D_2O-based miniemulsions[31,32] of a commercial poly(dimethylsiloxane), PDMS, M_n = 90 kDa, PD = 1.43, $M/M_e \approx 7$, $R_g \approx 8$ nm. Using dichloromethane as organic cosolvent to reduce the viscosity (and evaporating it afterward), we were able to realize average droplet sizes in the range of 200−1000 nm controlled by the surfactant (SDS) content, as confirmed by dynamic light scattering (Figure 1a) and cryo-TEM (data not shown). Note that the PDMS ^{1}H signal at around 0 ppm was in all cases well-resolved from the surfactant signals, allowing for a selective measurement of the PDMS component. No significant interpenetration and no absorptive interaction between the alkyl moieties of the surfactant, and the PDMS is expected. Importantly, in order to prevent rotational diffusion of the PDMS spheres from interfering with polymer dynamics on the same time scale, we tested different schemes of immobilization. While embedding in rigid poly(vinyl alcohol) after mixing with an aqueous solution and subsequent

*To whom correspondence should be addressed. E-mail: kay.saalwaechter@physik.uni-halle.de.

Published on Web 04/23/2010

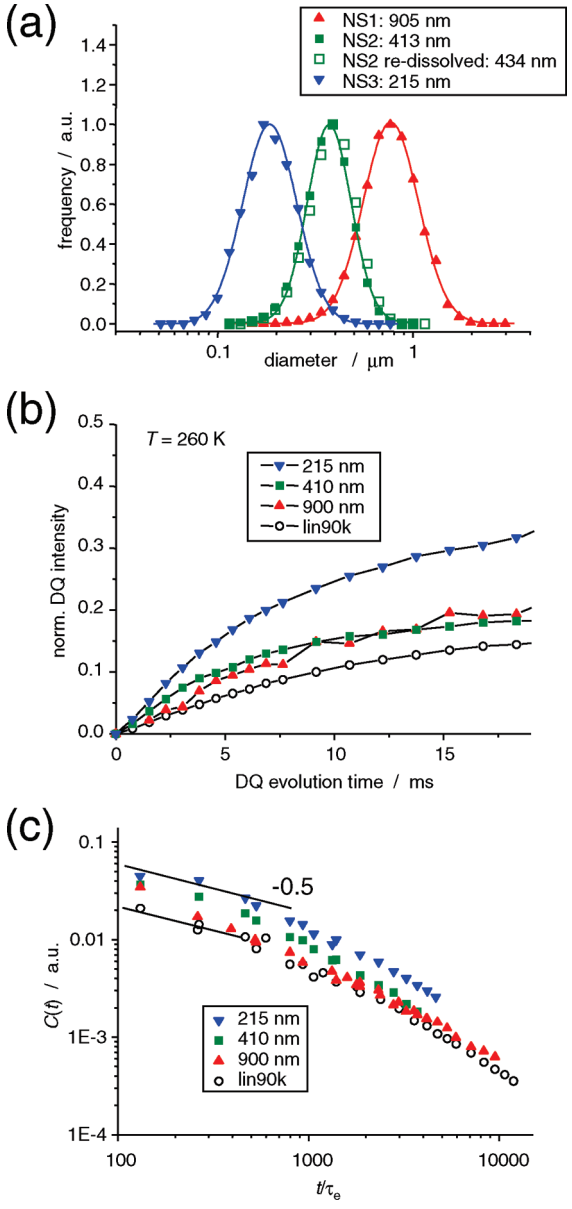

Figure 1. (a) Particle size distribution of PDMS miniemulsion droplets in D_2O, determined by dynamic light scattering. The redissolution result after solidification of the continuous phase with gelatin confirms the integrity of the spheres. (b) Normalized DQ build-up curves for PDMS in the bulk and confined to the different droplet sizes. (c) Orientation autocorrelation function $C(t/\tau_e)$ obtained after scaling analysis[23,26] of temperature-dependent DQ build-up data, referenced to $\tau_e(T)$ taken from the literature.[33,34]

evaporation did not preserve the integrity of the spheres, solidification of the water phase using 20 wt % gelatin worked well. Heating the gelled suspensions to about 50 °C and diluting in excess water confirmed the unchanged particle size distribution (see also Figure 1a).

Normalized DQ build-up data were obtained following published procedures.[24,25] The MQ experiment yields two τ_{DQ}-dependent signal functions, I_{DQ} and I_{ref}, where the latter is a decaying function representing at long times 50% of the overall main chain signal that does not evolve into DQ coherences. It also includes signals from less constrained segments such as chain ends, which are quantitatively identified as slowly relaxing singly exponential tails, often best in a representation of $I_{ref} - I_{DQ}$. After subtraction, the build-up rate of the normalized DQ intensity $I_{nDQ} = I_{DQ}/(I_{DQ} + I_{ref} - \text{tail})$ reflects the magnitude of anisotropic constraints imposed by topological constraints (entanglements) and relaxation due to motions on a time scale beyond τ_e.[23,24,26]

The nDQ build-up data plotted in Figure 1b immediately demonstrate that the chains in the smaller spheres are significantly constrained. Since a close-form analytical expression does not (yet) exist for a fit, we performed a scaling analysis proposed by Graf et al.,[23,26] which is based on the notion that in the short-time regime, $C(\tau_{DQ}) \propto I_{nDQ}(\tau_{DQ})/\tau_{DQ}^2$. Combining data taken at different temperatures, and shifting them using time−temperature superposition (TTS), based on the known temperature dependence of τ_e, we obtain an approximate $C(t/\tau_e)$, plotted in Figure 1c. We notice an initial power-law decay with an exponent of ~0.5, which indicates that the entanglement constraints are not yet fully developed at $M/M_e \approx 7$, in agreement with our recent results.[26] The limiting slope in the Doi−Edwards regime II would be 0.25.[26,35] The increasing slope toward longer times reflects the terminal relaxation, which appears to be unchanged in the differently confined systems. The only significant change is the overall upward shift of $C(t/\tau_e)$ by a factor of about 3, corresponding to a $\sqrt{3} \approx 1.7$-fold increase of the constraint-induced order.

It may be expected that this increase is not homogeneous across the melt droplet, yet the featureless nDQ data in these samples did not allow for any further conclusions. However, another very relevant observation concerns the separable signal tail of I_{ref}, which has been attributed to unentangled, isotropically moving chain ends. It presumably arises from contour-length fluctuation effects,[36] and in a bulk melt, it contributes to a decrease in elasticity by diluting the entangled fraction. Figure 2a shows sample fits of this tail fraction, and Figure 2b demonstrates its temperature dependence in all samples. In the bulk melt, it increases with temperature up to a range of 30%, which then roughly corresponds to the 2/7 fraction expected for the two outermost chain segments with lengths corresponding to M_e of a 7-fold entangled polymer chain. At lower temperatures, the chain dynamics is not fast enough to render the full M_e outer part isotropic on the NMR time scale.

Notably, this tail fraction decreases substantially in the confined samples, indicating that now even the chain ends experience anisotropic constraints; in other words, contour-length fluctuations appear to be suppressed. This may be rationalized by a (rather long-ranged) geometrically wall-induced anisotropy acting on top of the tube constraint. For a rough estimate of the range of such an effect, we can assume that the center parts of the droplets are bulklike and that the confined parts do not show isotropic chain-end signals at all. Under this crude assumption, one can estimate the amount of interphase-related polymer by scaling the bulk melt chain end fractions to fit the confined data (dashed lines in Figure 2b). Assuming that the confined fraction is located in a spherical outer shell of the droplets, the thickness of this shell is estimated to be 39 ± 8 nm, which is roughly 5 times the radius of gyration of the used PDMS.

The quantitative discussion of the results so far is subject to limitations, which are related to the use of a commercial PDMS with a non-negligible polydispersity of 1.4. Because of a rather large amount of material needed in the miniemulsion process, we did not attempt using more expensive monodisperse samples. Considering the width of the droplet size distributions (Figure 1a), and the general disadvantages of PDMS with its rather large M_e and its crystallization temperature in the 200 K range limiting the study of slower dynamics, we now turn to a better defined model system, namely the nanochannels in self-ordered anodic aluminum

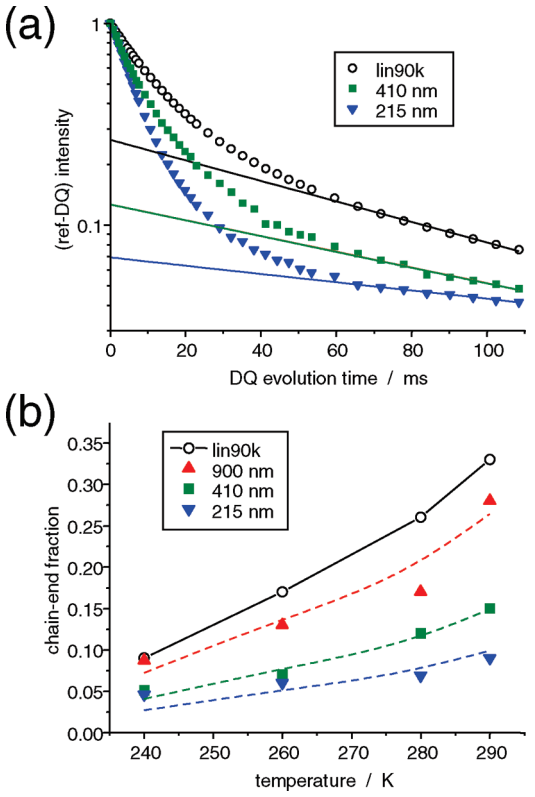

Figure 2. (a) Exponential signal tails related to isotropically mobile chain ends, as fitted to $I_{ref} - I_{DQ}$ for different PDMS samples at 280 K. (b) Chain-end fractions as a function of temperature for all PDMS samples. The dashed lines are interpolations of the bulk melt data, scaled down by factors of 0.8, 0.45, and 0.3 to match the confined-sample data.

oxide (AAO).[37] This system provides a hard-wall confinement imposed by hydroxyl-terminated surfaces saturated with water to different degrees depending on the applied annealing protocols. AAO can be infiltrated with unpolar polymers in the melt state, forming contiguous polymer nanorods[38] with rather neutral, noninteracting interfaces. This is important, as infiltration with (locally) polar polymers such as PDMS[39] or poly(ethylene oxide) would lead to nanometer-thick rigid absorption layers[40−42] and thus network-like constraints for the chains protruding from it.[43]

Nanoporous self-ordered AAO membranes, 100 μm in thickness, with pore diameters of 60 and 20 nm were infiltrated with monodisperse PB of M_n = 87 kDa, PD = 1.05, $M/M_e \approx 47$, and $R_g \approx 11$ nm. The time scale was estimated by simple mass uptake measurements (Figure 3b), which show that about 4 days are needed for complete infiltration. During this time, the samples exhibit a rather complex NMR behavior, as shown in Figure 3c. At low filling, the nDQ curves feature a quick initial rise, indicating a strongly confined fraction, which vanishes after more than 1 day of infiltration. In particular the response after only 0.5 h of infiltration suggests a superposition of signals from different microenvironments. A similar, allegedly layer-like behavior was in fact observed using commercially available AAO filter membranes (Whatman Anopore) partially filled with PDMS by solution infiltration.[44,45] Consistent with the mass uptake curve seen in Figure 3b, we observed an equilibrated response only after extended melt infiltration in excess of 1 day. Note that samples were repeatedly measured over periods of months after preparation, showing reproducible results. Initial nonequilibrium chain conformations are thus assumed to be well-annealed.

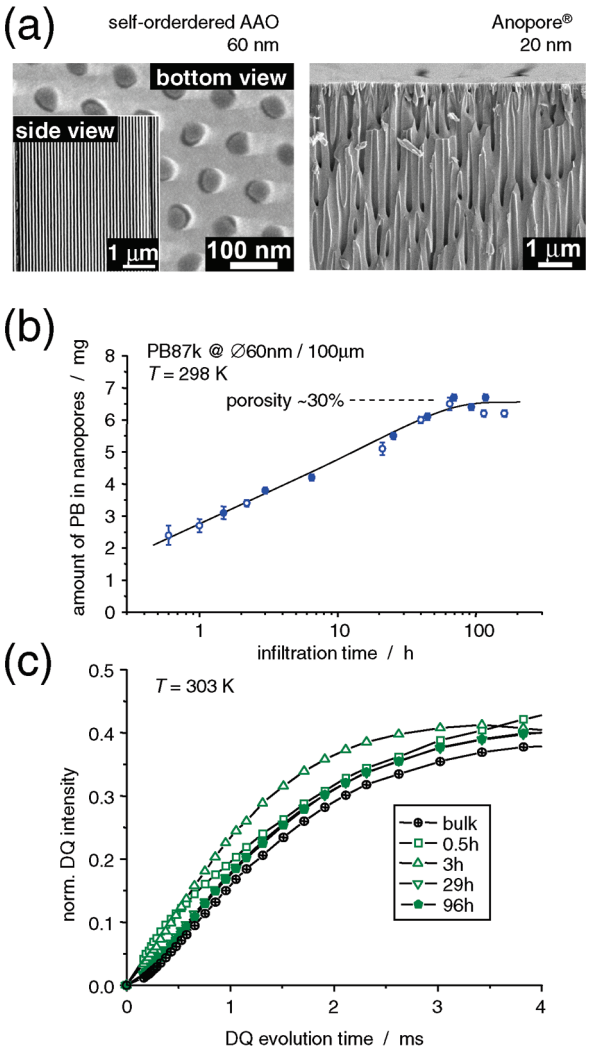

Figure 3. (a) Scanning electron micrographs of AAO. Left: bottom of a 100 μm thick self-ordered AAO membrane after infiltration with PB. The pore bottoms were opened by acid treatment, and the sample was coated with a thin gold layer. The complete filling of the pores with PB is obvious. Inset: cross section of a self-ordered AAO membrane prior to infiltration. Right: cross section of a disordered AAO filter membrane (Whatman Anodisc). (b) Infiltration kinetics at 298 K obtained from simple mass uptake measurements on two different samples, interrupted by removing and later adding again the bulk melt overlayer. (c) Normalized DQ build-up curves obtained at 303 K for samples after different infiltration times.

These results highlight the potential drawbacks inherent to the use of disordered AAO membranes in investigations of confined polymer dynamics. In particular, in commercially available AAO filter membranes, often only short pore segments actually exhibit the nominal pore diameter (see also Figure 3a). Moreover, without thorough identification of infiltration conditions yielding pores completely filled with equilibrated polymer melts, in particular in the presence of a volatile solvent, ill-defined and nonequilibrated states characterized by partial filling of the pore volume and a complex spatial distribution of the polymer may result. Some previous NMR results obtained on such samples should thus be handled with care,[44−46] also considering that the PDMS used in these studies is known to bind quite strongly to hydroxyl-terminated surfaces.[39]

Finally, we discuss the MQ NMR results obtained for PB confined to 20 and 60 nm wide nanochannels plotted in Figure 4. Because of the high number of entanglements per

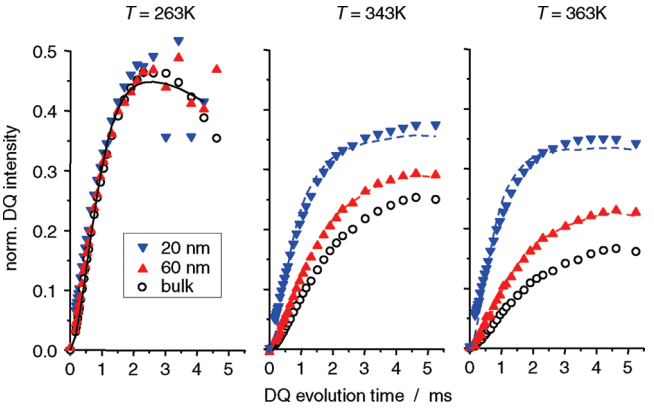

Figure 4. Normalized DQ build-up curves for PB in bulk and infiltrated into the nanochannels of self-ordered AAO at different temperatures. The solid line for 263 K is a fit demonstrating homogeneous entanglement constraints, and the dashed lines at higher temperatures are two-parameter fits yielding about 15 and 45% constrained network-like material in the 60 and 20 nm pores, respectively.

chain ($M/M_e \approx 47$), the isotropic end fraction is always <5% in these samples, and the determination of its content is subject to errors, which is why we refrain from a closer discussion at this point. Detailed studies are underway on samples with lower M. At the lowest temperature of 263 K, which is about 90 K above T_g (just as for the lowest temperature of our PDMS samples), we observe only little confinement effects (the 20 nm sample exhibits a somewhat quicker initial rise), which we explain with the dominance of the much stronger entanglement-induced anisotropy to chain motion. The response at 263 K is almost network-like as expected in the rubbery plateau (Doi−Edwards regime II), characterized by an intensity maximum close to 50%, and can be fitted to an apparent residual coupling on the order of $D_{res}/2\pi \approx 180$ Hz, which corresponds to a local order consistent with the entanglement spacing of this polymer.[26] At larger temperatures, local order in the bulk PB melt is reduced due to reptation, and the comparably quicker rise of the nDQ buildup of the AAO-confined PB directly reflects additional interface-induced anisotropy.

We observe qualitative differences to the soft-confined PDMS spheres, where the terminal dynamics appeared unaffected, leading to a monotonic decay of $C(t)$ (Figure 1c). Here, we were not able to obtain satisfactory representations of $C(t/\tau_e)$ using TTS, which we attribute to a more pronounced inhomogeneity of the response, affecting the shape of the $I_{nDQ}(\tau_{DQ})$ data at very early times, thus invalidating the $I_{nDQ}(\tau_{DQ}) \sim C(\tau_{DQ})\tau_{DQ}^2$ approximation. Further, the response in the 20 nm wide nanochannels is found to be only weakly temperature-dependent, indicating a network-like plateau in $C(t/\tau_e)$. At least for the associated confined fraction, the terminal relaxation does apparently not lead to isotropic chain motion in the long time limit, which may be explained by the different confinement geometry (straight long channel vs isotropic sphere).

A semiquantitative analysis is possible if we again make a simplifying assumption for the polymer in the surface layer. Here, we assume that the nDQ curves in confinement are superpositions of unchanged bulk-like material (for which we numerically interpolate the corresponding bulk data) and of a network-like component with a given residual coupling constant and no long-time relaxation (corresponding to an nDQ curve that reaches the long-time plateau at 50% intensity, such as the 263 K data in Figure 4). The dashed lines for the higher temperatures are two-parameter fits indicating 15 ± 2 and 45 ± 5% constrained material with $D_{res}/2\pi \approx 170 \pm 10$ and 260 ± 8 Hz for the 60 and 20 nm pores, respectively. The fit is somewhat inferior in the 20 nm pore, which is likely due to the existence of a more pronounced property gradient. The given intervals indicate the (weak) variation with temperature. The two fractions correspond to the same surface layer thickness of about 2.5 nm, which is now significantly less than R_g of this polymer.

In order to reconcile the different observations for PDMS and PB, we need to keep in mind that the estimates of the constrained fraction were based on different observations, respectively, i.e., missing isotropic chain-end parts (which were not significant for highly entangled PB) and the amount of polymer involved in significantly anisotropic segmental motion (which is too severely affected by terminal relaxation in lowly entangled PDMS). More conclusive results will be drawn from our ongoing study of a larger molecular-weight range and from an in-depth analysis of the experimental data. For now, we hypothesize that the length scale of geometrically induced anisotropy of segmental motion might be related to the entanglement separation (M_e) rather than the radius of gyration, explaining the rather large length scale of the effect observed for PDMS in the nanodroplets. This also makes sense from a more fundamental perspective, as the phenomena that we study (degree of anisotropy of the dynamics in Doi−Edwards regimes II and III) are governed by the entanglement density. Fast local motions, over which our NMR observable is averaged, are effectively restricted to a spatial domain governed by the entanglements, possibly limiting effects of geometric wall-induced anisotropy to this length scale.

A direct comparison of our observations with the "corset effect"[27−30] observed in terms of strong changes in frequency-dependent NMR T_1 relaxation times remains difficult as long as there is no molecular model predicting confinement-induced shape changes of the dipolar (orientation) autocorrelation function $C(t)$. Our results constitute a direct observation of the increase of the unaveraged part of the dipolar interaction tensor, corresponding to an increased (yet still small) absolute value of $C(t)$ at a time scale in the reptation regime of the bulk polymer (see ref 26 for details), while T_1 is also sensitive to faster motions down to the segmental level, reflecting the fluctuating part of the dipolar tensor, i.e., the decay of $C(t)$ toward the range that MQ NMR is sensitive to. The two methods are therefore complementary, and field-cycling T_1 investigations of our samples have thus been initiated. We note that the corset effect was reported to be homogeneous across the investigated samples, as evidenced by monoexponential T_1 relaxation, while we interpret the qualitative shape changes of our $I_{nDQ}(\tau_{DQ})$ data in terms of an inhomogeneous scenario.

Further, a recent inelastic neutron scattering study[47] focusing on fast segmental motions of poly(ethylene oxide) in self-ordered AAO channels of 40 nm diameter concluded no significant confinement effects on translational diffusion (apart from the expected immobilized absorption layer), which, however, as pointed out in a recent rebuttal by Kimmich and Fatkullin,[30] cannot be taken as evidence for the absence of a "corset effect" affecting rotational dynamics. Finally, the effect observed by us is significantly more pronounced than orientation effects described by Deloche and co-workers,[48] who did not detect any changes in moderately entangled PDMS films above 25 nm thickness. However, their effect in films below 25 nm could be quantitatively attributed to immediately geometrically induced segmental anisotropy in combination with diffusive averaging, and our preliminary T_2 relaxation experiments on macroscopically

ordered membrane stacks confirmed that the observed anisotropy is orientation-dependent, suggesting a similar origin of the phenomena.

Conclusions. We have found that geometric confinement leads to significantly more anisotropic chain fluctuations than predicted by the tube model on time scales beyond the entanglement time. In spherical confinement of PDMS melt droplets ($M/M_e \approx 7$), the average chain orientation is measurably increased, while the terminal dynamics (isotropization) appears unaffected, and the thickness of the confined material layer is estimated to about 40 nm, based on decreased isotropic chain-end signal. In contrast, cylindrical confinement of highly entangled PB ($M/M_e \approx 50$) leads to an almost temperature-independent response indicating network-like segmental anisotropy in an estimated ~3 nm surface layer. The differences may be due to the different confining geometries, and the rather different entanglement spacings of PDMS and PB, suggesting the tube diameter as the relevant length scale for the phenomenon.

While the overall phenomenon of increased segmental order is in tune with increased elasticity[19] and maybe also slowed-down diffusion[20−22] in some thin-film setups, it is an open question as to how our observations can be reconciled with the enhanced flow observed under more similar (weakly interacting interface) conditions.[15,17,18] A dominating effect of nonequilibrated chain conformations that are expected for these latter studies appears plausible. Further studies of PB in AAO nanochannels over a large molecular-weight range, self-diffusion measurements by pulsed-gradient NMR, more detailed infiltration experiments based upon confocal fluorescence microscopy of dye-doped polymers, and experiments focusing on changes in the interfacial properties by surface modification are underway and will be reported shortly.

Experimental Section. *Samples and Characterization.* The investigated PDMS base polymer was an alkyl-terminated PDMS obtained from Wacker Silicones, and the narrowly distributed PB (−H and −*sec*-butyl termination, about 54% *cis*, 41% *trans*, and 5% vinyl units) was purchased at PSS (Mainz, Germany). Other chemicals were obtained from Aldrich and used without further purification. The miniemulsions recipes were 1 g of PDMS, 4 g of dichloromethane, 20 g of D_2O, and 0.3−2.5 g of sodium dodecyl sulfate (SDS). First, a macroemulsion was prepared by vigorous stirring for 1 h, followed by ultrasonication (2 min at 120 W) using a Bandelin HD2200 with KE76 tip. Droplet size distributions were measured with a Horiba LA-920 particle sizer and confirmed by cryo-TEM. The emulsions were gelled by adding 20 wt % bone gelatin (Merck) at 50 °C. AAO membranes were prepared following the procedures reported in the literature.[37,49,50] Before infiltration, the AAO was dried in vacuum at 250 °C. Infiltration of PB into the membranes was performed by placing the PB on the surface of the AAO at 298 K under vacuum or argon atmosphere to prevent possible oxidation and subsequent removal of excess PB with a sharp blade. The aluminum substrate attached to the AAO layer was removed following procedures described elsewhere[51] prior to crushing and flame-sealing in evacuated NMR sample tubes.

NMR experiments on the PDMS nanospheres and the PB in AAO nanopores were performed on Bruker Avance 500 (B_0 = 11.7 T) and Bruker Avance II 400 (B_0 = 9.4 T) spectrometers, respectively, using in both cases the proton channel of standard Bruker static double-resonance probes. MQ experiments using a dedicated multipulse sequence were conducted and evaluated following previously published procedures.[25,26] For the experiments on PB infiltrated into AAO, broad signal components related to rigid surface hydroxyl groups and H-bonded water was suppressed by a MAPE dipolar filter[52] of 200 μs length prior the applying the MQ pulse sequence.

Acknowledgment. We are indebted to K. Landfester for her initial help with the preparation of the miniemulsions, to R. Thomann for cryo-TEM investigations, and to S. Kallaus and to K. Sklarek for the preparation of AAO. Constructive discussions with N. Fatkullin and R. Kimmich are gratefully acknowledged. Funding was provided by the DFG (SA982/4 and STE1127/9) in the priority programme SPP1369 "Polymer-Solid Contacts" as well as initially via the SFB428 (Freiburg).

References and Notes

(1) Keddie, J. L.; Jones, R. A. L.; Cory, R. A. Size-Dependent Depression of the Glass Transition Temperature in Polymer Films. *Europhys. Lett.* **1994**, *27*, 59–64.
(2) Baschnagel, J.; Binder, K. On the Influence of Hard Walls on Structural Properties in Polymer Glass Simulation. *Macromolecules* **1995**, *28*, 6808–6818.
(3) Lin, W.-Y.; Blum, F. D. Segmental Dynamics of Interfacial Poly(methyl acrylate)-d_3 in Composites by Deuterium NMR Spectroscopy. *J. Am. Chem. Soc.* **2001**, *123*, 2032–2037.
(4) Starr, F. W.; Schrøder, T. B.; Glotzer, S. C. Molecular Dynamics Simulation of a Polymer Melt with a Nanoscopic Particle. *Macromolecules* **2002**, *35*, 4481–4492.
(5) Alcoutlabi, M.; McKenna, G. B. Effects of confinement on material behaviour at the nanometre size scale. *J. Phys.: Condens. Matter* **2005**, *17*, R461–R524.
(6) Serghei, A.; Huth, H.; Schick, C.; Kremer, F. Glassy Dynamics in Thin Polymer Layers Having a Free Upper Interface. *Macromolecules* **2008**, *41*, 3636–3639.
(7) Serghei, A.; Kremer, F. Metastable States of Glassy Dynamics, Possibly Mimicking Confinement-Effect in Thin Polymer Films. *Macromol. Chem. Phys.* **2008**, *209*, 810–817.
(8) Peter, S.; Napolitano, S.; Meyer, H.; Wübbenhorst, M.; Baschnagel, J. Modelling Dielectric Relaxation in Polymer Glass Simulations: Dynamics in the Bulk and in Supported Polymer Films. *Macromolecules* **2008**, *41*, 7729–7743.
(9) Rittigstein, P.; Priestley, R. D.; Broadbelt, L. J.; Torkelson, J. M. Model polymer nanocomposites provide an understanding of confinement effects in real nanocomposites. *Nat. Mater.* **2007**, *6*, 278–282.
(10) Fakhraai, Z.; Forrest, J. A. Measuring the Surface Dynamics of Glassy Polymers. *Science* **2008**, *319*, 600–604.
(11) Jones, R. L.; Kumar, S. K.; Ho, D. L.; Briber, R. M.; Russell, T. P. Chain conformation in ultrathin polymer films. *Nature* **1999**, *400*, 146–149.
(12) Kraus, J.; Müller-Buschbaum, P.; Kuhlmann, T.; Schubert, D. W.; Stamm, M. Confinement effects on the chain conformation in thin polymer films. *Europhys. Lett.* **2000**, *49*, 210–216.
(13) Brûlet, A.; Boué, F.; Menelle, A.; Cotton, J. P. Conformation of Polystyrene Chain in Ultrathin Films Obtained by Spin Coating. *Macromolecules* **2001**, *101*, 4071–4097.
(14) Sen, S.; Xie, Y.; Kumar, S. K.; Yang, H.; Bansal, A.; Ho, D. L. Chain Conformations and Bound-Layer Correlations in Polymer Nanocomposites. *Phys. Rev. Lett.* **2007**, *98*, 128302.
(15) Shin, K.; Obukhov, S.; Chen, J.-T.; Huh, J.; Hwang, Y.; Mok, S.; Dobriyal, P.; Thiyagarajan, P.; Russell, T. P. Enhanged mobility of confined polymers. *Nat. Mater.* **2007**, *6*, 961–965.
(16) Si, L.; Massa, M. V.; Dalnoki-Veress, K.; Brown, H. R.; Jones, R. A. L. Chain Entanglement in Thin Freestanding Polymer Films. *Phys. Rev. Lett.* **2005**, *94*, 127801.
(17) Rowland, H. D.; King, W. P.; Pethica, J. B.; Cross, G. L. W. Molecular Confinement Accelerates Deformation of Entangled Polymers During Squeeze Flow. *Science* **2008**, *322*, 720–724.
(18) Barbero, D. R.; Steiner, U. Nonequilibrium Polymer Rheology in Spin-Cast Films. *Phys. Rev. Lett.* **2009**, *102*, 248303.
(19) Hu, H.-W.; Granick, S. Viscoelastic Dynamics of Confined Polymer Melts. *Science* **1992**, *258*, 1339–1342.
(20) Frank, B.; Gast, A. P.; Russell, T. P.; Brown, H. R.; Hawker, C. Polymer Mobility in Thin Films. *Macromolecules* **1996**, *29*, 6531–6534.
(21) Zheng, X.; Rafailovich, M. H.; Sokolov, J.; Strzhemechny, Y.; Schwarz, S. A.; Sauer, B. B.; Rubinstein, M. Long-Range Effects

on Polymer Diffusion Induced by a Bounding Interface. *Phys. Rev. Lett*. **1997**, *79*, 241–244.
(22) Pu, Y.; Rafailovich, M. H.; Sokolov, J.; Gersappe, D.; Peterson, T.; Wu, W.-L.; Schwarz, S. A. Mobility of Polymer Chains Confined at a Free Surface. *Phys. Rev. Lett*. **2001**, *87*, 206101.
(23) Graf, R.; Heuer, A.; Spiess, H. W. Chain-Order Effects in Polymer Melts Probed by ^{1}H Double-Quantum NMR Spectrocopy. *Phys. Rev. Lett*. **1998**, *80*, 5738–5741.
(24) Saalwächter, K.; Heuer, A. Chain Dynamics in Elastomers as Investigated by Proton Multiple-Quantum NMR. *Macromolecules* **2006**, *39*, 3291–3303.
(25) Saalwächter, K. Proton Multiple-Quantum NMR for the Study of Chain Dynamics and Structural Constraints in Polymeric Soft Materials. *Progr. NMR Spectrosc*. **2007**, *51*, 1–35.
(26) F. Vaca Chávez K. Saalwächter. NMR Observation of Entangled Polymer Dynamics: Tube Model Predictions and Constraint Release. *Phys. Rev. Lett*., in press.
(27) Fatkullin, N.; Fischer, E.; Mattea, C.; Beginn, U.; Kimmich, R. Polymer Dynamics under Nanoscopic Constraints: The "Corset Effect" as Revealed by NMR Relaxometry and Diffusometry. *ChemPhysChem* **2004**, *5*, 884–894.
(28) Fatkullin, N.; Kimmich, R.; Fischer, E.; Mattea, C.; Beginn, U. The confined-to-bulk dynamics transition of polymer melts in nanoscopic pores of solid matrices with varying pore diameter. *New J. Phys*. **2004**, *6*, 46.
(29) Kausik, R.; Mattea, C.; Fatkullin, N.; Kimmich, R. Confinement effect of chain dynamics in micrometer thick layers of a polymer melt below the critical molecular weight. *J. Chem. Phys*. **2006**, *124*, 114903.
(30) Kimmich, R.; Fatkullin, N.; . The corset effect, field-cycling NMR relaxometry, transverse NMR relaxation, field-gradient NMR diffusometry, and incoherent neutron scattering. *J. Chem. Phys. 132*, in press.
(31) Landfester, K. The Generation of Nanoparticles in Miniemulsions. *Adv. Mater*. **2001**, *13*, 765–768.
(32) Landfester, K. Miniemulsions for Nanoparticle Synthesis. *Top. Curr. Chem*. **2003**, *227*, 75–123.
(33) Ferry, J. D. *Viscoelastic Properties of Polymers*; John Wiley: New York, 1980.
(34) Mark, J. E., Ed.; *Physical Properties of Polymers Handbook*; Springer: New York, 2007.
(35) Doi, M.; Edwards, S. F. *The Theory of Polymer Dynamics*; Clarendon Press: Oxford, 1986.
(36) Kimmich, R.; Köpf, M.; Callaghan, P. Components of Transverse NMR Relaxation in Polymer Melts: Influence of Chain-End Dynamics. *J. Polym. Sci., Part B: Polym. Phys*. **1991**, *29*, 1025–1030.
(37) Masuda, H.; Fukuda, K. Ordered Metal Nanohole Arrays Made by a Two-Step Replication of Honeycomb Structures of Anodic Alumina. *Science* **1995**, *268*, 1466–1468.
(38) Zhang, M.; Dobriyal, P.; Chen, J.-T.; Russell, T. P.; Olmo, J.; Merry, A. Wetting Transition in Cylindrical Alumina Nanopores with Polymer Melts. *Nano Lett*. **2006**, *6*, 1075–1079.
(39) Cohen-Addad, J. P.; Roby, C.; Sauviat, M. Characterization of chain binding to filler in silicone−silica systems. *Polymer* **1985**, *26*, 1231–1233.
(40) Litvinov, V. M.; Zhdanov, A. A. Molecular Motions in Filled Polydimethylsiloxanes. *Vysokomol. Soedin., Ser. A* **1987**, *29*, 1021–1027.
(41) Kirst, K. U.; Kremer, F.; Litvinov, V. M. Broad-Band Dielectric Spectroscopy on the Molecular Dynamics of Bulk and Adsorbed Poly(dimethylsiloxane). *Macromolecules* **1993**, *26*, 975–980.
(42) Sato, A.; Knoll, W.; Pennec, Y.; Djafari-Rouhani, B.; Fytas, G.; Steinhart, M. Anisotropic propagation and confinement of high frequency phonons in nanocomposites. *J. Chem. Phys*. **2009**, *1330*, 111102.
(43) Şerbescu, A.; Saalwächter, K. Particle-induced network formation in linear PDMS filled with silica. *Polymer* **2009**, *50*, 5434–5442.
(44) Primak, S. V.; Jin, T.; Dagger, A. C.; Finotello, D.; Mann, E. K. Chain segment order in ultrathin polymer films: A deuterium NMR study. *Phys. Rev. E* **2002**, *65*, 031804.
(45) Jagadeesh, B.; Demco, D. E.; Blümich, B. Surface induced order and dynamic heterogeneity in ultra thin polymer films: A ^{1}H multiple-quantum NMR study. *Chem. Phys. Lett*. **2004**, *393*, 416–420.
(46) Ayalur-Karunakaran, S.; Blümich, B.; Stapf, S. NMR investigations of polymer dynamics in a partially filled porous matrix. *Eur. Phys. J. E* **2008**, *26*, 43–53.
(47) Krutyeva, M.; Martin, J.; Arbe, A.; Colmenero, J.; Mijangos, C.; Schneider, G. J.; Unruh, T.; Su, Y.; Richter, D. The Role of Internal Rotational Barriers in Polymer Melt Chain Dynamics. *Macromolecules* **2002**, *35*, 4198–4203.
(48) Rivillon, S.; Auroy, P.; Deloche, B. Chain Segment Order in Polymer Thin Films on a Nonabsorbing Surface: A NMR Study. *Phys. Rev. Lett*. **2000**, *84*, 499–502.
(49) Masuda, H.; Hasegwa, F.; Ono, S. Ordered Metal Nanohole Arrays Made by a Two-Step Replication of Honeycomb Structures of Anodic Alumina. *J. Electrochem. Soc*. **1997**, *144*, L127–L130.
(50) Li, A. P.; Müller, F.; Birner, A.; Nielsch, K.; Gösele, U. Hexagonal pore arrays with a 50420 nm interpore distance formed by self-organization in anodic alumina. *J. Appl. Phys*. **1998**, *84*, 6023–6026.
(51) Hohlbein, J.; Steinhart, M.; Schiene-Fischer, C.; Benda, A.; Hof, M.; Hübner, C. G. Confined Diffusion in Ordered Nanoporous Alumina Membranes. *Small* **2007**, *3*, 380–385.
(52) Mauri, M.; Thomann, Y.; Schneider, H.; Saalwächter, K. Spin Diffusion NMR at Low Field for the Study of Multiphase Solids. *Solid State Nucl. Magn. Reson*. **2008**, *34*, 125–141.